

# Effect of carrier gas composition on transferred arc metal nanoparticle synthesis

Matthias Stein · Dennis Kiesler ·  
Frank Einar Kruis

Received: 27 September 2012 / Accepted: 22 December 2012 / Published online: 10 January 2013  
© Springer Science+Business Media Dordrecht 2013

**Abstract** Metal nanoparticles are used in a great number of applications; an effective and economical production scaling-up is hence desirable. A simple and cost-effective transferred arc process is developed, which produces pure metal (Zn, Cu, and Ag) nanoparticles with high production rates, while allowing fast optimization based on energy efficiency. Different carrier gas compositions, as well as the electrode arrangements and the power input are investigated to improve the production and its efficiency and to understand the arc production behavior. The production rates are determined by a novel process monitoring method, which combines an online microbalance method with a scanning mobility particle sizer for fast production rate and size distribution measurement. Particle characterization is performed via scanning electron microscopy, energy-dispersive X-ray spectroscopy, and X-ray diffraction measurements. It is found that the carrier gas composition has the largest impact on the particle production rate and can increase it with orders of magnitude. This appears to be not only a result of the increased heat flux and melt temperature but also of the formation of tiny nitrogen (hydrogen) bubbles in the molten feedstock, which

impacts feedstock evaporation significantly in bi-atomic gases. A production rate of sub 200 nm particles from 20 up to 2,500 mg/h has been realized for the different metals. In this production range, specific power consumptions as low as 0.08 kWh/g have been reached.

**Keywords** Metal nanoparticles · Transferred arc · Online characterization · Energy efficiency

## Introduction

The interest in pure metal nanoparticles has increased significantly over the past years, as well as their number of applications. Owing to their characteristic attributes, metal nanoparticles are used in optoelectronics, medicine, sensor technology, information storage, and catalysis (Feldheim and Foss 2001). The increasing demand from the industry for metal particles therefore challenges scientists and engineers around the world to develop processes, which are easily scalable and produce a product with adequate purity. Numerous methods to synthesize metal nanoparticles are known, but especially plasma synthesis has the potential to produce high-quality nanoparticles economically and in large quantities.

The term plasma synthesis comprises a great variety of processes and applications, which differ already in their approach. In general, one can divide plasmas into thermal plasmas (in local thermal

M. Stein (✉) · D. Kiesler · F. E. Kruis  
Institute for Nanostructures and Technology (NST) and  
Center for Nanointegration Duisburg-Essen (CENIDE),  
University of Duisburg-Essen, Bismarckstr.81, 47057  
Duisburg, Germany  
e-mail: matthias.stein@uni-due.de  
URL: www.uni-due.de/nst

equilibrium, LTE) and nonthermal plasmas (not in LTE), based on the temperature ratio between electrons and ions as well as their number densities (Griem 1964; Tendero et al. 2006). Both systems are widely used to produce nanoparticles. Nonthermal plasma synthesis has been used for example by Kortshagen (2009) or Mariotti and Sankaran (2010). But, especially in terms of the process economy of scaling-up, thermal plasmas appear more promising. Thermal plasmas have been studied intensively (Fauchais and Vardelle 1997; Pfender 1999; Heberlein 2002; Tendero et al. 2006). They are used under atmospheric or reduced pressure to produce nanoparticles and can be subdivided into radiofrequency (RF) plasmas (Boules et al. 2011; Kobayashi et al. 2007), thermal microwave plasmas (Brenner et al. 1997; Vollath 2008), spark discharges (Weber et al. 2001; Roth et al. 2004; Tabrizi et al. 2009), or DC discharges. DC discharges are used in non-transferred arc processes also known as plasma jets or plasma sprays (Schütze et al. 1998; Heberlein et al. 2001; Fukumasa and Fujiwara 2003; Fauchais 2004; Seo and Hong 2012) or in transferred arc processes (Mahoney and Andres 1995; Mahoney et al. 1996; Chen et al. 2006), where the direct striking of the arc on the anode is fundamental.

However, only few plasma synthesis methods are suitable for scaling-up the production rate. Some processes have a low energy efficiency, demand a too large investment, or are unsuitable simply because the produced particles are not any more nanoscaled when increasing the production rate. A promising method to increase the production rate of metal nanoparticles economically is the transferred arc synthesis, where a lot of effort has already been done to optimize and scale-up the production of metal nanoparticles.

Mahoney et al. (1995, 1996) have developed a transferred arc process synthesizing nanoparticles of metals, metal oxides, nitrides, or carbides. The material evaporation is realized by arc evaporation, which is ignited by contacting of the electrodes and separating them to an arc gap of  $\sim 0.5$  cm. It is found that the evaporation rate can be controlled by the applied current (10–70 A), which on the other hand affects the voltage (8–13 V) and thereby the energy input. Evaporation rates up to 50 g/h are reported, but no actual production rates presented. Depending on the gas flow rate in the arc- and quench-region, particle sizes of 1–100 nm have been achieved. Chen et al. (2006) have presented a simple and versatile mini-arc

plasma source for nanocrystal synthesis. The arc is ignited by contact between a tungsten cathode and a graphite crucible anode via a commercial TIG welder. Owing to the design of the crucible, the arc parameters are independent from the feedstock material. At an electrode distance of 0.5 mm, the arc is fed by 30–40 A at  $\sim 3$  V. Silver nanoparticles of 60 nm with a mass production rate of up to 10 mg/h were synthesized. Celik et al. (2002) have described a transferred arc method for the production of ultrafine powder of any conductive material, such as metals, alloys, ceramics, etc. A process with high evaporation rates (0.5 kg/h) has been achieved to synthesize pure particles mostly of 1  $\mu\text{m}$ . Wei et al. (2006) have generated copper nanoparticles by their transferred arc process, which show high purity, single phase, and spherical shape. Haidar (2009) has used a transferred arc to produce aluminum and aluminum oxide nanoparticles in a low pressure system. Cole et al. (2009) have synthesized positively charged gold or zinc oxide nanoparticles by arc discharge to build well-positioned three-dimensional nanostructures. Uda et al. (1983) have increased the production rate of fine metal particles via transferred arc by adding hydrogen to the carrier gas (argon). Among others, silver and aluminum particles smaller than 1 micron are synthesized using 25 % hydrogen and 75 % argon as carrier gas. With an energy input of ca. 4,500 W, 0.04 g/h aluminum and 42 g/h silver are generated. Munz et al. (1999) have used a transferred arc to synthesize silica and aluminum nitride. It is shown that hydrogen addition to argon increases the silica production. Tanaka et al. (1987) explained the enhanced evaporation of feedstock material by the addition of hydrogen or nitrogen to argon in a transferred arc due to the formation of small hydrogen (nitrogen) bubbles in metallic silicon. Those bubbles are capable of transporting additional silicon atoms to the top of the melt and thereby increase the production rate. They have found that hydrogen bubbles are less effective to form bigger bubbles and hence to provide less material than nitrogen bubbles due to the faster atomic hydrogen diffusion in the melt. A production rate enhancement of manganese-silver alloy nanoparticles by hydrogen addition in a transferred arc discharge due to tiny hydrogen bubble formation is also reported by Lee et al. (2010). Shin and Park (2010) have found that the addition of nitrogen to argon as quench gas increases the evaporation of

copper powder. Based on a comparison of the evaporation rate of a transferred arc plasma system to a non-transferred plasma torch system they concluded that the transferred arc system is better suited for the production of nanopowders from bulk material than the non-transferred arc system. Förster et al. (2012) have presented an experimental study on the production of copper nanoparticles with a transferred arc. In a slightly subatmospheric argon system, a 70–120 A transferred arc is ignited between a tungsten rod cathode and a graphite crucible anode filled with copper to be evaporated. Copper particles in the size range of 4–50 nm are synthesized, depending on arc current, arc length, gas flows, and hydrogen addition to the sheath gas. Especially, the stability of the process over 8 h is notable. Table 1 summarizes some of the important parameters of the previously discussed publications.

A lot of modeling efforts have been directed toward the understanding of different process parameters. Especially, the following publications have helped to understand the influence of the carrier gas on the arc and accordingly the production rate, which is one of the main goals of this work.

Murphy et al. (2009) have investigated the influence of the gas composition in TIG welding. It is found that adding hydrogen, nitrogen, or helium to argon leads to an increase in the heat flux density to the anode and, therefore, the weld pool depth and size. The temperature increase is explained by the greater arc constriction due to the thermal pinch effect and also by the increase of the thermal conductivity. Lim et al. (2008) have shown that the removal of impurities in copper by plasma arc melting is improved when

adding 20 % hydrogen to argon. This is explained by an increased surface temperature of the copper because of the hydrogen presence. Ramirez-Argaez et al. (2009) have performed mathematical modeling to study the influence of different gases on high-intensity electric arcs. It is shown that nitrogen has a high arc power because of its small electric conductivity and hence increased electric resistance. It is observed to be almost the opposite for argon arcs, where the good electric conductivity leads to low power arcs. A review of the effects of metal vapor in arc welding is given by Murphy (2010). It is concluded that even low metal concentrations strongly affect two thermophysical properties: the net radiative emission coefficient and the electrical conductivity. In general, the presence of metal vapor increases the electrical conductivity, the current density and thereby the heat flux density of the plasma. Metal vapor also increases the radiative emission coefficient across the full range of temperatures in the arc which leads to a cooling of this region. Both effects lead to a decrease in the arc temperature. Furkawa et al. (2002) have investigated the effect of copper vapor on the heat transfer in a nitrogen plasma. The heat transfer, generally caused by convection, impact of electrons on the anode and radiation is found to decrease with increasing concentration of metal vapor. Their simulations show that the metal vapor increases the electrical conductivity in the plasma and therefore decreases the thermal conductivity and temperature of the plasma. The heating efficiency of a molten anode is 20 % smaller than that of a solid anode. Li et al. (2008) have calculated that silver vapor in an arc with air as carrier gas has a stronger cooling effect than copper vapor at the arc

**Table 1** Summary of process parameters of transferred arc processes (\* reactive synthesis)

Author	$P$ (W)	Material	$Q_{\text{Carrier}}$ (l/min)	$Q_{\text{Quench}}$ (l/min)	Carrier gas
Celik et al.	24,500	Cu, Ni	60	300	Ar, H <sub>2</sub>
Chen et al.	120	Ag, SnO <sub>2</sub> *	5	1.5	Ar, Air*
Cole et al.	10	Au, Zn	–	–	Air
Förster et al.	<1,350	Cu	2–4	6	Ar, H <sub>2</sub>
Lee et al.	<5,280	Mn–Al	–	–	Ar, H <sub>2</sub>
Mahoney et al.	<910	In, TiN*, TiO <sub>2</sub> *	5–10	0–12	Ar, O <sub>2</sub> *, N <sub>2</sub> *
Munz et al.	<14,000	AlN	(15)	–	Ar, H <sub>2</sub> , NH <sub>3</sub> *
Shin and Park	13,500	Cu	10–260	50	Ar, N <sub>2</sub>
Tanaka et al.	<2,000	Si	–	–	Ar, H <sub>2</sub> , N <sub>2</sub>
Uda et al.	<4,500	Fe	–	–	Ar, H <sub>2</sub>
Wei et al.	–	Cu	–	–	Ar

center and a clearer restriction effect on the arc motion.

In this work, an improved transferred arc process is developed which produces pure metal nanoparticles with high production rates while allowing a rapid optimization for energy efficiency to insure environmental sustainability. The main goal of this work is to determine the influence of the carrier gas composition on production rate and energy efficiency. Different plasma gases are investigated. As shown in Table 1, a lot of work especially on high-power arc synthesis has been done; however, to the best of the authors' knowledge, the influence of carrier gases on actual metal nanoparticle production rates has been investigated only marginally. The study of Tanaka et al. (1987) showed a clear influence of the carrier gas composition for transferred arc synthesis of silicon. The scarcity of investigations of metal nanoparticles is probably caused by the general avoidance of nitrogen, which can lead to nitride formation. However, in nitride-forming systems, such as silicon, the nitride is not necessarily formed, as it dissociates at high temperatures in the arc (Tanaka et al. 1987). Especially for metal particles there are metals not forming nitrides, for which an investigation of nitrogen arc synthesis is interesting. According to the simulations of Murphy et al. (2009), nitrogen does not only offer a higher temperature arc but also lower costs for gas consumption than argon. This investigation concentrates on finding optimal conditions for highly efficient metal nanoparticle production, using a low-cost reactor setup as well as an off-the-shelf power supply operating with power <math><1\text{ kW}</math>. A novel process monitoring method has been developed, which bases on a rapid dilution followed by online process aerosol characterization. This consists of continuous measurement of the mass concentration using a tapered element oscillating microbalance (TEOM) and a fast measurement of the particle size distribution based on the equivalent mobility diameter using a scanning mobility particle sizer (SMPS). From the mass concentration measurement, the production rate can be directly determined. Offline particle characterization is performed by means of a scanning electron microscopy (SEM), Energy-dispersive X-ray spectroscopy (EDX), and X-ray diffraction (XRD) measurements. In the following, the experimental setup and procedure are shown and the investigated various parameters presented, before the results are presented and discussed.

## Experimental setup

The overall experimental setup is shown in Fig. 1. The heart of the setup is the reactor chamber in which metal evaporation and particle formation takes place. It has a double-walled construction which allows water-cooling. It consists of a DN 160 ISO-K chamber, containing 5 circumferentially placed ISO-KF 40 ports, which can be used either for adaptive gas inlets (process or quenching gas), aerosol outlet, electrode arrangements, monitoring tools or feeding mechanisms (Fig. 2). A mass flow controller adjusts the desired carrier gas flow (3.5–10 l/min) into the reactor chamber. As carrier gas argon, helium, nitrogen, or 95 % nitrogen + 5 % hydrogen is used. All gases have a purity of at least 5.5. The nitrogen is additionally cleaned using a purifier (Alphagaz Purifier O<sub>2</sub>-Free, Air Liquide, Düsseldorf, Germany). The electrode pair consists of a tungsten rod cathode and a graphite crucible acting as anode, in which the material to be evaporated is filled. The electrode distance is set between 3 and 7 mm, depending on feedstock material, carrier gas composition, and gas flow. The crucible is not cooled with the purpose to minimize energy losses and to keep the reactor chamber as simple as possible. The material to be evaporated is filled into a cylindrical recess with a diameter of 20 mm and a depth of 10 mm machined at the end of a massive graphite rod. The graphite rod has also a reduced diameter in its middle part to reduce the heat losses toward the current feedthrough. Copper, silver, and zinc initially in the form of 5-mm spherical shots are used because they are easy to handle, especially for re-feeding the crucible. As can be seen in Fig. 2, different electrode arrangements with respect to the gas flow have been investigated: a cross-flow setup (Fig. 2a) and an axial-flow setup (Fig. 2b). The carrier gas is fed perpendicular toward the arc in the cross-flow setup. The gas flow enters the system by a 4-mm inner diameter ceramic tube placed at a distance of 10 mm from the crucible. An upward flow over the axis of the anode is realized in the axial setup with the cathode placed perpendicular to the gas above the crucible.

The reactor chamber can be evacuated to 0.5 mbar using a vacuum pump (Adixen ACP 15, Pfeiffer Vakuum GmbH, Wertheim, Germany). The pressure is monitored using a vacuum transducer (910 Dual-Trans, MKS Inst. Corp., Andover, MA, USA). By

refilling, re-evacuating, and again filling the system with the carrier gas, the oxygen concentration inside the chamber is reduced as much as possible. The process pressure is atmospheric.

Two ports of the reactor chamber are used for the power supply connection, where a cost-effective power supply, a TIG welding generator (AC/DC Tig-Liner 210P, Schweisstechnik Klinger, Gladbeck, Germany) with a maximum current of 210 A is used. The electric connection is fed into the chamber by vacuum feedthroughs (max. 150 A, 5 kV). One is directly contacted to the graphite crucible by a crucible carrier in form of a titanium rod with a diameter of 12 mm, adjustable in height by a micrometer screw. The carrier is made of grade 1 titanium

having relatively low heat conductance, while maintaining good electrical conductivity. The other feedthrough is connected to a 1.6-mm tungsten rod which serves as the cathode. The tungsten cathode can be adjusted such that the arc is ignited centrally above the crucible. It is also not cooled.

Particles formed by the atomic vapor created by the arc evaporation via condensation and coagulation are carried away from the reactor and characterized online or offline. For offline measurements, particles are deposited either on a TEM-grid via electrostatic precipitation (Dixkens and Fissan 1999) for STEM measurement (JSM 7500F, Jeol, Tokyo, Japan) or on a PTFE filter with a pore size of 5 μm for gravimetric or XRD measurement (X'pert Pro MPD with Ni-filtered

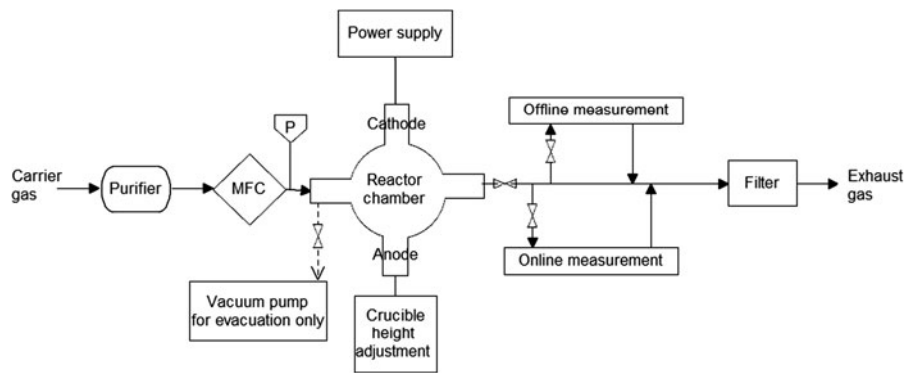


**Fig. 1** Experimental setup

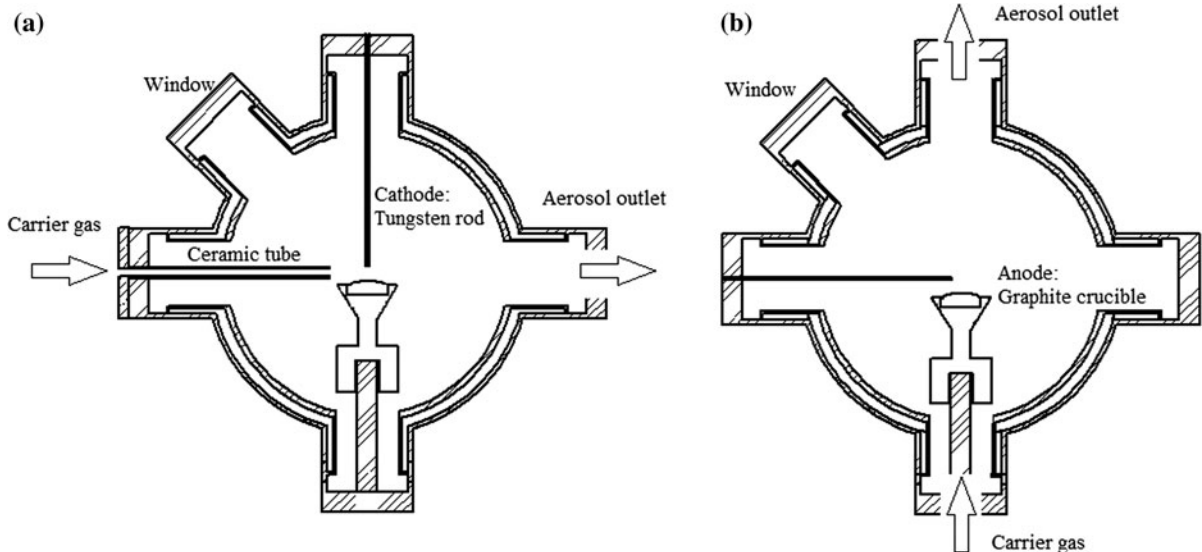


**Fig. 2** Schematic of the reactor: **a** cross-flow setup and **b** axial-flow setup. Carrier gas flow is indicated by arrows

copper  $K\alpha$  radiation, PANalytical, Almelo, Netherlands). The filter is suitable for XRD measurements of metals since it does not show any diffraction peaks at angles below  $20^\circ$ . The data are recorded in steps of  $2\theta = 0.01^\circ$  over a range of  $20^\circ \leq 2\theta \leq 120^\circ$ .

Online measurements are made by aerosol characterization methods which necessitate, however, moderate particle number concentrations so that a dedicated dilution system is required. An aerosol dilution system with a maximum dilution ratio of 1,000 is used (VKL 10 + VKL 100 Cascade System, Palas, Karlsruhe, Germany). A part of the product flow is sampled into the dilution system as a result of the reduced pressure created in an ejector and diluted with the ejector gas. This is repeated in the second stage ejector-diluter and then passed to the measurement equipment (Fig. 3). An SMPS system consisting of a neutralizer, a Differential Mobility Analyzer (DMA 3081, TSI, Minneapolis, MN, USA), a particle counter (CPC 3775, TSI), and a controller (Classifier 3080, TSI), is used to measure the aerosol size distribution based on the equivalent mobility diameter. The particle mass concentration in the product flow is measured using a TEOM (Series 1405, Thermo Fisher Scientific, Waltham, MA, USA) which measures the particle mass deposited in a filter placed on an oscillating microbalance. The production rate can then be calculated with the help of the total flow of

aerosol as well as the dilution ratio. Therefore, actual production rates are measured online and not derived from evaporation rates.

In this study, the production rate is determined on the basis of the mass loading of the aerosol downstream of the reactor. Owing to the significant losses to the walls, this production rate is lower than the actual evaporation rate. The particle losses are for all material systems similar so we assume that the production rate reflects the evaporation rate.

## Results and discussion

### Influence of gas composition

It is known that the gas composition has a marked influence on the arc power and thereby the evaporation of material. Especially, hydrogen addition to argon arcs has been investigated in the past to increase the evaporation rate of material (Uda et al. 1983; Munz et al. 1999; Lee et al. 2010; Förster et al. 2012). To the best of the authors' knowledge, other gas compositions, such as described in the following, have not been investigated with the goal to increase the nanoparticle production rate and thereby improve the process economy and energy efficiency.

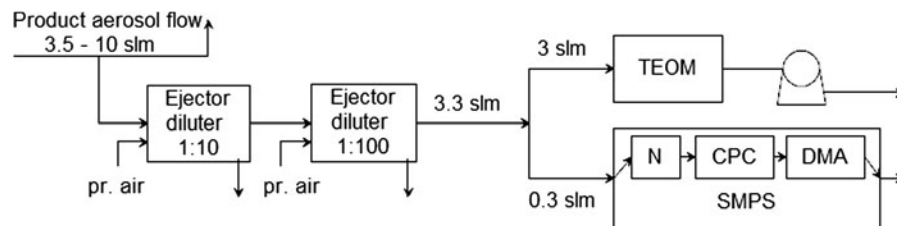


**Fig. 3** Online measurement by TEOM and SMPS with ejector-dilution system

**Table 2** Influence of different argon gas mixtures on important arc parameters

Carrier Gas	Thermal conductivity (W/(m K))	Electric conductivity (A/(V m))	Heat flux density (W/mm <sup>2</sup> )	Current density (A/mm <sup>2</sup> )	Arc pressure (Pa)
Ar	2.3	7.5	50	7.2	275
Ar + 10 vol.% He	2.4	7.3	55	7.3	280
Ar + 10 vol.% N <sub>2</sub>	2.6	7.3	63	9.5	370
Ar + 9 vol.% H <sub>2</sub>	3	7.2	90	10.9	440

Data taken from Murphy et al. (2009)

According to Murphy et al. (2009), the important arc parameters influenced by the gas composition are the heat flux density, current density, and arc pressure near the anode, which can lead to an increase in anode temperature and thereby directly influencing the evaporation rate. Table 2 shows the results of their numerical simulations of an arc between a tungsten cathode and a water-cooled copper anode for different gases mixed with argon. The heat flux and current density, which probably have the highest influence on the melt heating and evaporation, increase significantly in ascending order, when helium, nitrogen, or hydrogen is added even at the moderate concentrations around 10 % used in this study.

In the present process, the production rate behaves as expected in accordance to the calculations of Murphy for argon and helium carrier gases, which show an increase of thermal conductivity, heat flux density, current density, and arc pressure. In our experiments (Fig. 4), more zinc is produced than silver and copper in agreement with its much higher vapor pressure (for zinc  $10^3$  mbar at 1,200 K, for silver  $10^{-3}$  mbar, for copper  $10^{-5}$  mbar; Honig and Kramer 1969). The change from an argon to a helium arc increases the particle production rate of all three metals approximately by factor 5 at constant electric current. From the investigated gases, argon has the highest electric conductivity and lowest heat capacity, which leads to a broad, but comparatively low power arc (Ramirez-Argaez et al. 2009). Hence, less material is evaporated.

When nitrogen is used as carrier gas, the heat flux and current density at the anode is larger, the arc power

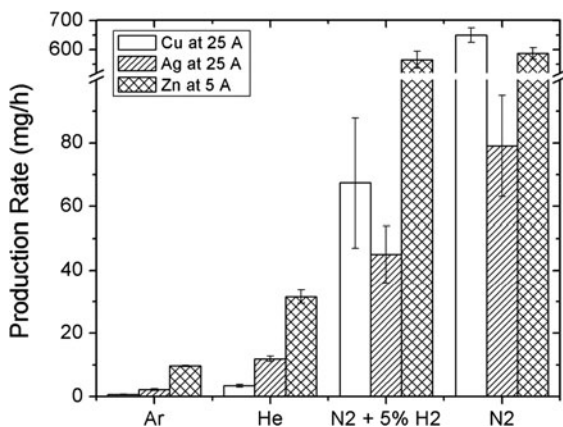


**Fig. 4** Dependence of the gas composition on the production rate for copper, silver (both 25 A), and zinc (5 A) in the cross-flow arrangement

and therefore the evaporation rate increase. However, the enormous increase in production rate is not caused by the enhanced thermal evaporation alone. Tanaka et al. (1987) observed a significant increase in production rate of silicon nanoparticles when adding nitrogen to an argon arc. They concluded that molecular nitrogen dissociates completely at high arc temperatures leading to an extremely high partial pressure of atomic nitrogen in the arc. On the other hand, nitrogen atoms recombine outside the arc to form molecular nitrogen, maintaining a low atomic nitrogen partial pressure. The steady recombination of atomic nitrogen generates more heat that can be used for material evaporation. This effect can only occur in a bi-atomic gas, such as nitrogen or hydrogen. Also, a mechanically caused increase in production rate is described due to the formation of small bubbles in the molten feedstock containing nitrogen, which splash fine molten feedstock material when moving to the surface outside of the arc. The movement of those bubbles is also explained by the difference in partial pressure of the nitrogen. This effect has also been observed by Lee et al. (2010) for manganese aluminum alloys and Förster et al. (2012) for copper, when adding hydrogen to an argon arc. In this study, all production rates increase further, when changing from a pure helium to a pure nitrogen arc (Fig. 4), but not in accordance to the vapor pressure of the metals. The production rate of copper in nitrogen is 100 times higher in comparison to the one of copper in helium. A significant increase in particle production by a factor of 20 is also observed for zinc. The production rate of silver, however, increases only by a factor of 5 so that the production rate of copper particles now exceeds the one of silver.

An explanation for the smaller increase in production rate of silver in comparison to copper is difficult to find and might be a consequence of different effects. XRD measurements indicate crystalline zinc, silver, and copper with all carrier gases with minimal oxygen contaminations. Figure 5 shows the XRD pattern when nitrogen is used as carrier gas. Crystalline metal oxides are not detected. The significant increase in copper evaporation in nitrogen can be observed visually through the observation window. The change from an argon arc to a nitrogen arc leads to a broader, bright green-lighting arc. The weld pool in the crucible expands, but remains shallow. However, the copper is molten only partially and not liquid to the bottom of

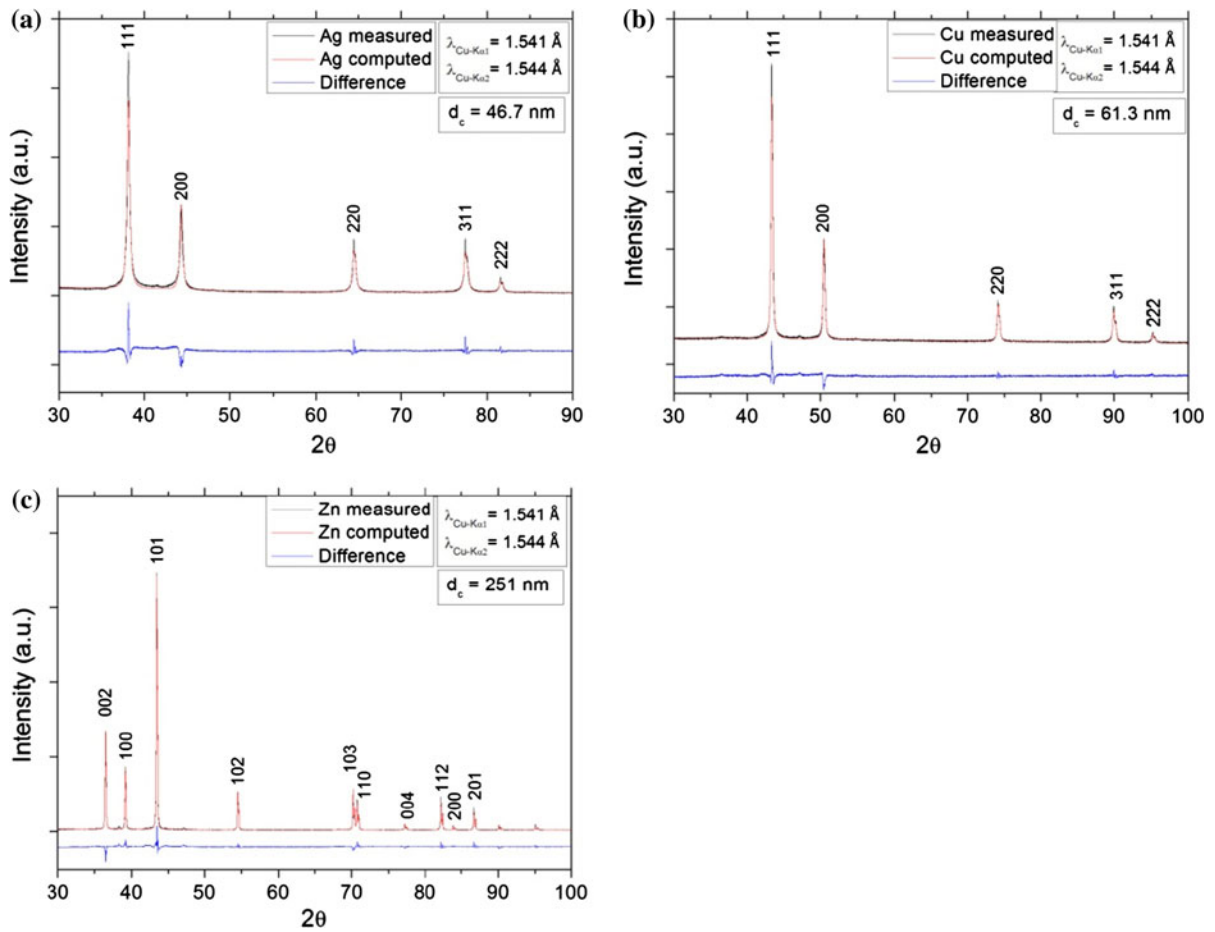


**Fig. 5** XRD pattern for Ag (a), Cu (b), and Zn (c) synthesized in a nitrogen plasma (3.5 slm N<sub>2</sub>) (cross-flow adjustment).  $d_c$  is the calculated crystalline size of the metal particles (Lutterotti 2010)

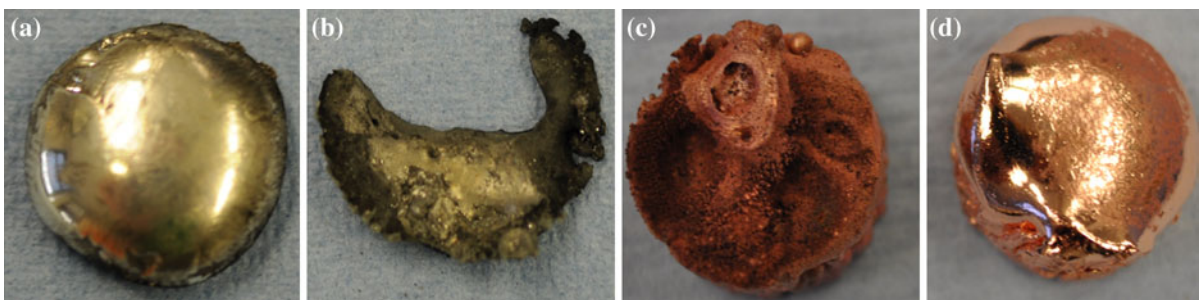


**Fig. 6** Congealed feedstock of a silver, b zinc, c copper after arc evaporation in nitrogen atmosphere, and d copper after arc evaporation in nitrogen + 5 % hydrogen atmosphere

the crucible. Figure 6 shows the shallow congealed copper (c) with cavities and almost spherical shaped silver (a) feedstock material. Huge cavities are observable on the congealed copper, which are assumed to be a result of the nitrogen bubble formation

described above. This is not observed for silver. In the nitrogen arc, the molten silver takes an almost spherical shape. It is completely liquid in the crucible. The spherical shape of the silver melt is conserved when the arc is extinguished and the silver congeals.



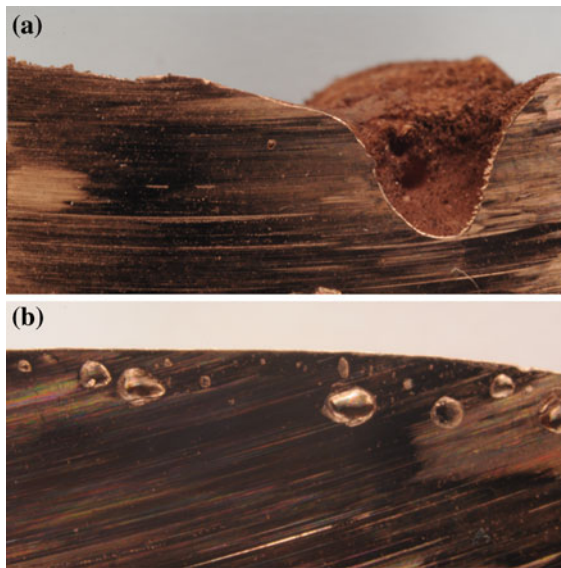


**Fig. 7** Section photograph of the congealed copper feedstock after **a** pure nitrogen arc processing and **b** nitrogen + 5 % hydrogen processing

No cavities are observable. It appears that the formation of tiny nitrogen bubbles in silver is suppressed, which might be a consequence of the decreased diffusion of nitrogen in silver in contrast to copper. For zinc (b), almost no material remains after processing even for short times, due to the fast evaporation. EDX measurements have been performed on the congealed silver and copper to investigate the composition of the feedstock material after synthesis. Both materials show relics of tungsten and oxygen on the surface of the melt so one can conclude that the feedstock composition is not responsible for the different evaporation behavior. During synthesis, a copper oxide layer on the melt would directly evaporate due to the higher vapor pressure in comparison to pure copper (Mack et al. 1923). The tungsten relics appear to behave as a kind of slag on the melt since they are mainly detected at the edge of both samples. This might explain also why no tungsten impurities are detected by XRD in the particles.

The nitrogen arc also appears smaller in case of the silver. The arc shape and attachment to the anode seems to influence the evaporation remarkably. Nonetheless, the reason for the difference in arc attachment is not understood. Metal vapor may influence the evaporation rate of the anode material. It is reported that even low concentration of metal vapor can increase the electrical conductivity, and therefore

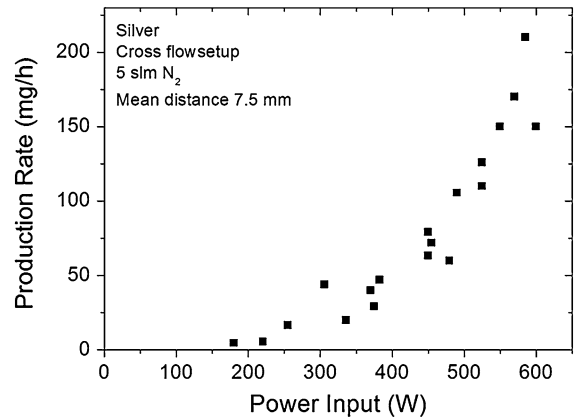


**Fig. 8** Production rate of silver nanoparticles as a function of power input, synthesized in a cross-flow setup with 5 slm  $N_2$

lowers the arc power (Etemadi and Pfender 1985; Furkawa et al. 2002; Murphy 2010). A decreased evaporation may result. That copper vapor, in comparison to silver vapor, leads to a difference in those conductivities at low concentrations is, however, unlikely.

The production rate of copper, silver (both at 25 A), and zinc (5 A) in a carrier gas composed of 5 % hydrogen in nitrogen is also displayed in Fig. 4. The production rate of copper particles is higher than the one of silver in the nitrogen + 5 % hydrogen mixture, but is smaller than the one in a pure nitrogen atmosphere. In view of the larger heat flux and current density predicted by Murphy (2010) for the hydrogen mixture as compared to the nitrogen mixture, this is not expected. Figure 6 displays the congealed copper feedstock after nitrogen (c) and nitrogen + 5 % hydrogen (d) processing. As can be seen, the feedstock shape changes significantly due to the hydrogen addition. The copper melts completely. Almost no visible cavities appear. The congealed copper shows a shiny surface as it is the case for the congealed silver after nitrogen processing. This may confirm the impact of the absorption of nitrogen (hydrogen) into the molten feedstock and the formation of small bubbles, which increase the production rate. A section photograph of the congealed copper feedstock after nitrogen (a) and 5 % hydrogen mixture (b) is shown in Fig. 7. In the nitrogen sample, huge cavities appear at the surface of the feedstock. In contrast to this, no cavities are visible at the surface of the hydrogen sample, but small bubbles appear inside the sample. This observation is confirmed by the hypothesis that hydrogen bubbles are less effective to

**Fig. 9** Dependence of arc voltage and power input on applied electric current and electrode gap distance (voltage) with copper electrodes (5 slm, cross-flow setup, nitrogen)

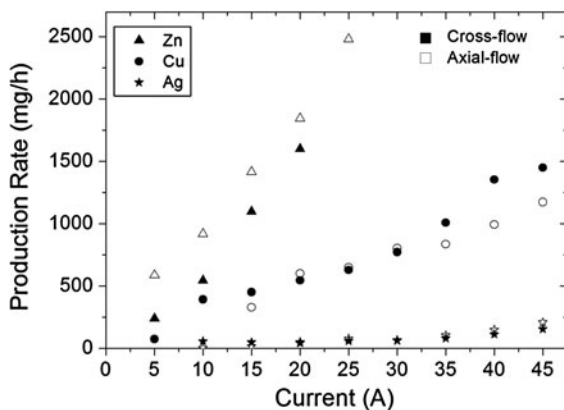
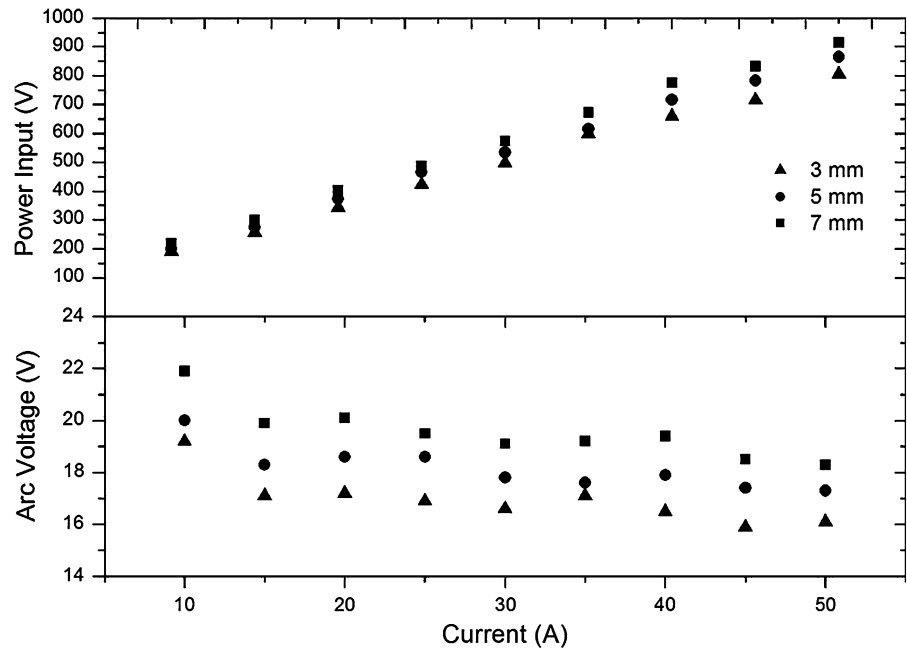


**Fig. 10** Comparison of production rate for cross-flow and axial-flow setup for three different metals in a nitrogen arc at a flow rate of 5 slm

form bigger bubbles than nitrogen, which might be a consequence of the faster diffusion of hydrogen atoms in the molten feedstock (Tanaka et al. 1987). Smaller bubbles splash less material. Accordingly, the splashing material appears to have a greater effect on the production rate than the increased feedstock temperature since for copper the particle production rate in the nitrogen + 5 % hydrogen arc is a factor of 13 smaller than that in a pure nitrogen arc.

However, the splashing of nitrogen bubbles might lead to the formation of micron-sized particles, which

affect the production rate significantly. SEM measurements show some micron-sized particles directly after the reactor, but much less in front of the measurement equipment. This may be the consequence of several bends in the aerosol line from the reactor to the measurement zone and the dilution system, where micron-sized particles may impact. Especially at those bends, particle depositions are observed so one can conclude that the effect of the micron-sized particles on the production rate is not only that significant but also not negligible and will be part of future investigations.

Since the effect of bubble formation is a consequence of the dissociation and recombination of bi-atomic molecular gases, they seem more suitable for arc evaporation than atomic gases. It is remarkable that the atomic gases behave as expected in terms of production rate opposed to the bi-atomic molecular gases, which cannot be predicted by Murphy's model as it does not include the bubble formation.

#### Influence of power input

It is well known that the power input can be used as a controlling parameter for material evaporation in a transferred arc (Mahoney and Andres 1995; Celik et al. 2002; Wei et al. 2006). This effect is also visible in the nanoparticle production rate (Fig. 8) since it increases

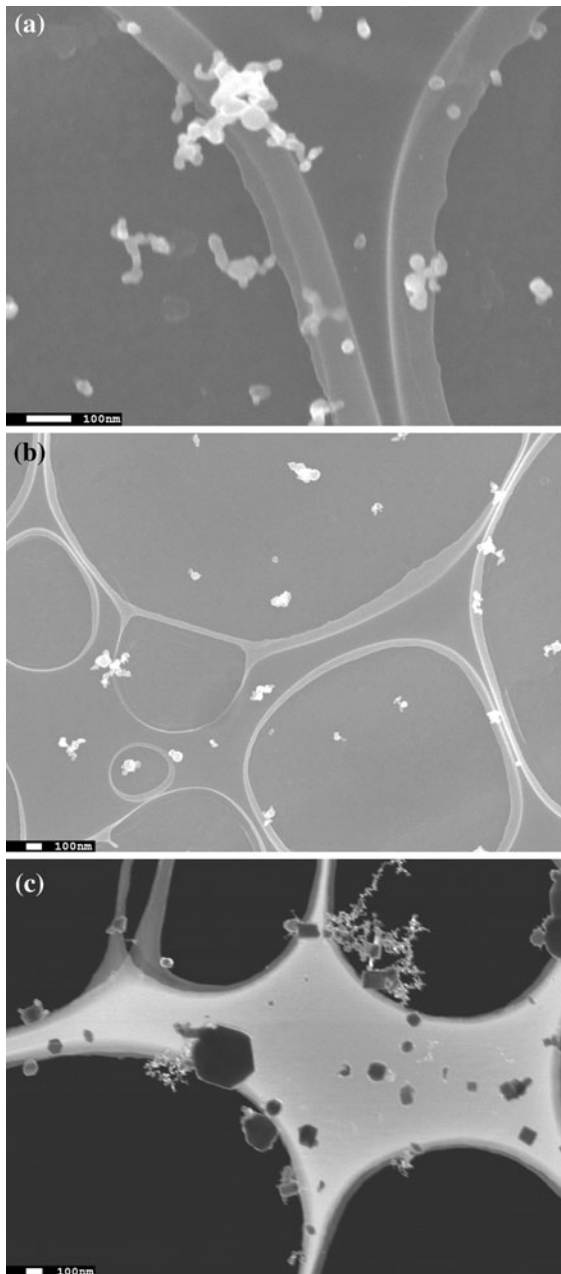


**Fig. 11** SEM images of silver (a), copper (b), and zinc (c) synthesized in cross-flow arrangement with 3.5 slm  $N_2$  at 50 A

strongly with power input above a threshold value for the investigated power range. For silver, there is a minimum power input of 175 W required to start feedstock evaporation and particle formation. The higher the power of the arc, the more energy is directed to the anode and hence to the material to be evaporated.

While a higher energy input increases the temperature and thereby the evaporation of material and the particle production rate, it as well increases the energy costs for the system. Figure 9 displays the dependence of the arc voltage and the input power on the applied current and the electrode distance. The power input is calculated from the product of the applied electric current and the resulting voltage between the electrodes. However, the required voltage for a stable arc decreases slightly with increasing current.

The investigation above shows that a nitrogen arc has a significant higher production rate than the other investigated arcs. Therefore, nitrogen has been used for the investigation of the influence of the power input on the particle production rate. Figure 10 displays the production rate for the three investigated metals and the two setups shown in Fig. 2. As can be seen, with increasing electric current, the production rate rises. The production rate differs for the metals. Zinc has the lowest vapor pressure, therefore shows the highest material evaporation and particle production rate. As discussed above, the production rate of copper particles exceeds the one of silver in a nitrogen arc by a factor  $>10$ . In a nitrogen atmosphere, 50 mg silver, 700 mg copper, and 2,500 mg zinc are synthesized per hour at an applied electric current of 25 A. A change in the electrode arrangement does not lead to a significant improvement. While the production rate for zinc and silver is slightly higher in the axial-flow setup, for copper, the cross-flow setup seems more productive at higher currents. In the cross-flow setup, the gas flow is directly guided toward the arc, and therefore, to the particle nucleation zone. Hence, the impact of the gas flow on the particle size is found to be greater so that the particle size control is easier. The axial setup on the other hand has the advantage of a much more stable arc, which is especially for lower electric currents and the lower energetic arcs such as the argon arc useful. Since arc synthesis is a highly thermal process, upward gas flow in the same direction as the buoyancy may lead to less wall deposition and thereby higher process efficiency, as less turbulences and smaller temperature gradients occur.

The increase in production rate is reflected by an increase in primary particle size and crystallite size, as determined by SEM and XRD. SEM measurements of electrostatically precipitated particles show agglomerates for all synthesized metals (Fig. 11). While the primary particle size can be determined from these images and compared with the XRD measurements above, the agglomerate size is also indicated by the

SMPS measurements. The results of the size measurements are summarized in Table 3. In nitrogen, the primary particle size of copper is about 65 nm which is 20-nm larger than the ones of silver. Although the agglomerate size is almost similar in both systems, the difference in primary particle size leads to a significant larger mass in case of copper. Zinc particles are even bigger, crystallite diameters appear which cannot be determined by means of XRD, and therefore lead to the largest particle production rate. By the addition of quench gas, lowering the input power or increasing the flow rate the particle size can be reduced (Shin and Park 2010; Förster et al. 2012), but this has not been the focus of this investigation.

For both setups, significant particle losses have been observed. The evaporation rate in the axial-flow setup is approximately 10 times higher than the detected particle production rate. For the cross-flow setup, these losses are similar with ca. 90 %. Most of the lost particles are found at the water-cooled reactor wall, which allows to collect them from the wall (e.g., by liquid) and thereby increase the particle yield. First measurements with an improved axial setup show a significant reduction in particle losses by the extension of the aerosol outlet KF 40 tube. To increase the aerosol particle production further, a guided aerosol flow inside the reactor chamber may be corrective and is part of future work.

### Specific power consumption

The strong influence of the carrier gas on the production rate directly impacts the specific power consumption (Fig. 12). Since the highest production rate has been reached in a nitrogen arc, its specific power consumption is the lowest for all three metals. The nitrogen + 5 % hydrogen mixture, helium, and argon follow in ascending order for all investigated metals.

**Table 3** Comparison of primary particle-/crystallite- size and agglomerate-/electrical mobility size at maximum production rate (50 A for copper and silver, 25 A for zinc)

	Primary particle size (nm)	Crystallite size (nm)	Agglomerate size (nm)	Electrical mobility diameter (nm)
	SEM	XRD	SEM	SMPS
Cu	65	61	80–150	98
Ag	45	47	60–160	102
Zn	80–400	–	100–600	–

Zinc has the lowest specific power consumption due to its high vapor pressure. The consumption ranges between 0.1 and 10 kWh/g and is below 1 kWh/g at 25 A for all gases tested. For copper, it is only for the nitrogen arc below 1 kWh/g for the other gases one or two orders of magnitude higher. It is noticeable that the specific power consumption of copper is virtually independent of the electric current for all gases. The specific power consumption of silver is similar to that of copper, except for the case of nitrogen, where it shows increased values between 3 and 10 kWh/g. In contrast to copper, the specific power consumption of silver is not independent of the electric current but slightly decreasing. This decrease is due to the production rate which in case of silver increases exponentially (Fig. 8), whereas it depends linearly on the electric current in case of copper. It appears that the development of the specific power consumption with power input is strongly material dependent.

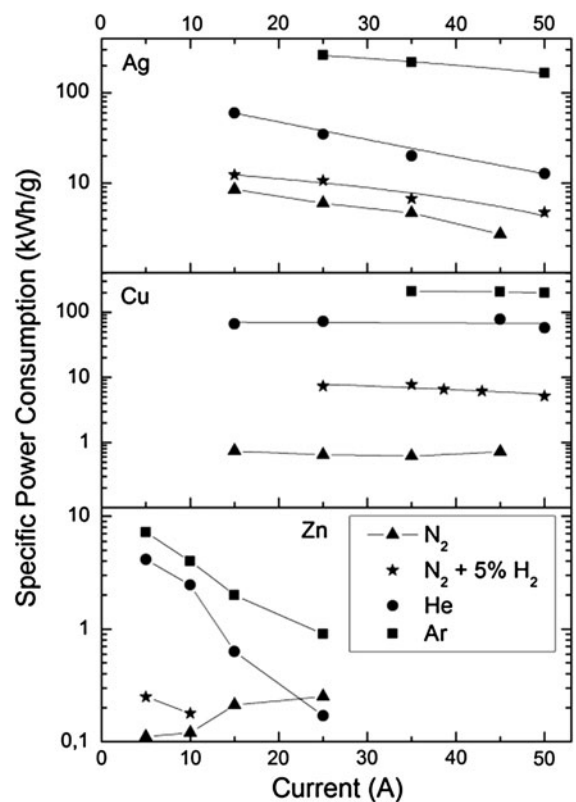


**Fig. 12** Specific power consumption for Ag, Cu and Zn depending on applied electric current and carrier gas composition

## Conclusion

A highly simplified and cost-effective production process by means of a transferred arc with relatively low power input (<1 kW) has been developed, including a novel process monitoring method for fast production rate and particle size distribution determination. Pure metal nanoparticles down to a size of 45 nm and a production rate from 20 mg/h up to 2,500 mg/h have been realized for different metals. In this production range, specific power consumptions as low as 0.08 kWh/g have been reached. The production rate increases with the applied electric current and is thereby easily controllable, which can be explained by an increase of arc power, anode region temperature and thereby stronger material evaporation. It is found that the carrier gas composition has the largest impact on the particle production rate and can increase it with orders of magnitude. This increase is observed for all investigated metals. In argon and helium, the evaporation rate increases when metals with a higher vapor pressure are used. In the nitrogen arc, copper particle production exceeds the one of silver, although the vapor pressure of copper is lower. This appears to be a consequence of the formation of tiny nitrogen bubbles in the molten feedstock, which impacts feedstock evaporation significantly in bi-atomic gases. The addition of hydrogen to the nitrogen carrier gas does not lead to an increase of production rate, since the bubble formation is reduced for hydrogen, due to the faster hydrogen diffusion in the molten feedstock. Two setups have been investigated; however, in terms of production rate, it appears that the arrangement of electrodes to gas flow influences the production rate and specific power consumption only slightly. It can be concluded that for metals not forming nitrides, the nitrogen arc is by far the most energy-efficient process.

**Acknowledgments** The research leading to these results has received funding from the European Union's Seventh Framework Program under grant agreement No. 280765 (BUONAPART-E).

## References

- Boules MI, Jurewicz J, Guo J (2011) Induction plasma synthesis of nanopowders. US patent No. 8013269 B2
- Brenner JR, Harkness JBL, Knickelbein MB, Krumdick GK, Marshall CL (1997) Microwave plasma synthesis of carbon-supported ultrafine metal particles. *Nanostruct Mater* 8:1–7
- Celik C, Addona T, Boulos MI, Chen G, Davis HJ (2002) Method and transferred arc plasma system for production of fine and ultrafine powders. United States Patent No. 6379419 B1
- Chen J, Lu G, Zhu L, Flagan RC (2006) A simple and versatile mini-arc plasma source for nanocrystal synthesis. *J Nanopart Res* 9:203–212
- Cole JJ, Lin EC, Barry CR, Jacobs H (2009) Continuous nanoparticle generation and assembly by atmospheric pressure arc discharge. *Appl Phys Lett* 95:113101
- Dixkens J, Fissan H (1999) Development of an electrostatic precipitator for off-line particle analysis. *Aerosol Sci Technol* 30:438–453
- Emadi K, Pfender E (1985) Impact of anode evaporation on the anode region of a high-intensity argon arc. *Plasma Chem Plasma Process* 5(2):175–182
- Fauchais P (2004) Understanding plasma spraying. *J Phys D Appl Phys* 37:86–108
- Fauchais P, Vardelle A (1997) Thermal plasmas. *IEEE Trans Plasma Sci* 25(6):1258–1280
- Feldheim DL, Foss CA (2001) Metal nanoparticles: synthesis, characterization, and applications. Decker, New York City
- Förster H, Wolfrum C, Peukert W (2012) Experimental study of metal nanoparticle synthesis by an arc evaporation/condensation process. *J Nanopart Res* 14(7):1–16
- Fukumasa O, Fujiwara T (2003) Rapid synthesis of ferrite particles from powder mixtures using thermal plasma processing. *Thin Solid Films* 435:33–38
- Furukawa S, Amakawa T, Adachi K (2002) Effects of copper vapor on heat transfer from atmospheric nitrogen plasma to a molten metal anode. *Plasma Chem Plasma Process* 22(1):85–104
- Griem HR (1964) Plasma spectroscopy. McGraw-Hill, New York
- Haidar J (2009) Synthesis of Al nanopowders in an anodic plasma. *Chem Plasma Process* 29:307–319
- Heberlein J (2002) New approaches in thermal plasma technology. *Pure Appl Chem* 74(3):327–335
- Heberlein J, Postel O, Girshick S, McMurry P, Gerberich W, Iordanoglou D, Di Fonzo F, Neumann D, Gidwani A, Fan M, Tymiak N (2001) Thermal plasma deposition of nanophas hard coatings. *Surf Coat Technol* 142–144:265–271
- Honig RE, Kramer DA (1969) Vapor pressure data for the solid and liquid elements. *RCA Rev* 30:285–305
- Kobayashi N, Kawakami Y, Kamada K, Li JG, Ye R, Watanabe T, Ishigaki T (2007) Spherical submicron-size copper powders coagulated from a vapor phase in RF induction thermal plasma. *Thin Solid Films* 516:4402–4406
- Kortshagen U (2009) Nonthermal plasma synthesis of semiconductor nanocrystals. *J Phys D Appl Phys* 42(11):113001
- Lee JG, Li P, Choi CJ, Dong XL (2010) Synthesis of Mn–Al alloy nanoparticles by plasma arc discharges. *Thin Solid Films* 519:81–85
- Li X, Chen D, Li R, Wu Y, Niu C (2008) Electrode evaporation effects on air arc behavior. *Plasma Sci Technol* 10(3):323–327
- Lim JW, Kim MS, Munirathnam NR, Le MT, Uschikoshi M, Mimura K, Isshiki M, Kwon HC, Choi GS (2008) Effect of Ar/Ar-H<sub>2</sub> plasma arc melting on Cu purification. *Mater Trans* 49(8):1826–1829

- Lutterotti L (2010) Total pattern fitting for the combined size-strain-stress-texture determination in thin film diffraction. *Nuclear Instrum Meth B* 268:334–340
- Mack E, Osterhof GG, Kraner HM (1923) Vapor pressure of copper oxide and of copper. *J Am Chem Soc* 45(3):617–623
- Mahoney W, Andres RP (1995) Aerosol synthesis of nanoscale clusters using atmospheric arc evaporation. *Mater Sci Eng A204*:160–164
- Mahoney W, Kempe MD, Andres RP (1996) Aerosol synthesis of metal and metal oxide nitride and carbide nanoparticles using an arc evaporation source. *Mat Res Soc Symp Proc* 400:65–70
- Mariotti D, Sankaran RM (2010) Microplasmas for nanomaterials synthesis. *J Phys D Appl Phys* 43(32):323001
- Munz RJ, Addona T, da Cruz AC (1999) Application of transferred arcs to the production of nanoparticles. *Pure Appl Chem* 71(10):1889–1897
- Murphy AB (2010) The effect of metal vapour in arc welding. *J Phys D Appl Phys* 43:434001
- Murphy AB, Tanaka M, Tashiro S, Sato T, Lowke JJ (2009) A computational investigation of the effectiveness of different shielding gas mixtures for arc welding. *J Phys D Appl Phys* 42:115205
- Pfender E (1999) Thermal plasma technology: where do we stand and where are we going? *Plasma Chem Plasma Process* 19(1):1–31
- Ramirez-Argaez MA, Gonzalez-Rivera C, Trapaga G (2009) Mathematical modeling of high intensity electric arcs burning in different atmospheres. *ISIJ Int* 49(6):796–803
- Roth C, Ferron GA, Karg E, Lentner B, Schumann G, Takenaka S, Heyder J (2004) Generation of ultrafine particles by spark discharging. *Aerosol Sci Technol* 38:228–235
- Schütze A, Jeong JY, Babayan SE, Park J, Selwyn GS, Hicks RF (1998) The atmospheric-pressure plasma jet: a review and comparison to other plasma sources. *IEEE Trans Plasma Sci* 26(6):1685–1694
- Seo JH, Hong BG (2012) Thermal plasma synthesis of nano-sized powders. *Nuclear Eng Technol* 44(1):9–20
- Shin MG, Park WD (2010) Synthesis of copper nanopowders by transferred arc and non-transferred arc plasma systems. *J Optoelectron Adv Mater* 12(3):528–534
- Tabrizi NS, Ullmann M, Vons VA, Lafont U, Schmitt-Ott A (2009) Generation of nanoparticles by spark discharge. *J Nanopart Res* 11(2):315–332
- Tanaka K, Ishizaki K, Yumoto S, Egashira T (1987) Production of ultra-fine silicon powder by the arc plasma method. *J Mater Sci* 22:2192–2198
- Tendero C, Tixier C, Tristant P, Desmaison J, Leprince P (2006) Atmospheric pressure plasmas: a review. *Spectrochim Acta B* 61:2–30
- Uda M, Ohno S, Hoshi T (1983) Process for production fine metal particles. United States Patent No. 4376740
- Vollath D (2008) Plasma synthesis of nanopowders. *J Nanopart Res* 10:39–57
- Weber AP, Seipenbusch M, Kasper G (2001) Application of aerosol techniques to study the catalytic formation of methane on gasborne nickel particles. *J Phys Chem A* 105:8958–8963
- Wei Z, Xia T, Ma J, Dai J, Feng W, Wang Q, Yan P (2006) Growth mechanism of Cu nanopowders prepared by anodic arc plasma. *Trans Nonferr Met Soc China* 16:168–172